

Plasmon wake in anisotropic two-dimensional materials

Zoran L. Mišković¹ and Milad Moshayedi

Department of Applied Mathematics, University of Waterloo, Waterloo, Ontario N2L 3G1, Canada

 (Received 24 April 2023; accepted 24 July 2023; published 25 August 2023)

We use analytically tractable dielectric response models, which are supported by *ab initio* calculations for anisotropic two-dimensional (2D) materials and quasi-2D metals that host slow plasmons, to reveal a rich variety of the plasmonic wake patterns in the electric potential induced by a charged particle moving parallel to those materials. Using the method of stationary phase, we discover surprising analogies with Kelvin's ship wakes and atmospheric wakes regarding the asymmetry of the wake, slowing down of the plasmon dispersion, and the onset of Mach-like wake due to nonlocal effects in the dielectric response.

DOI: [10.1103/PhysRevResearch.5.033133](https://doi.org/10.1103/PhysRevResearch.5.033133)

I. MOTIVATION

The wave pattern trailing behind a ship that moves at constant speed v on a straight-line trajectory on deep, calm water is a ubiquitous phenomenon known as the ship wake, first described mathematically by Lord Kelvin [1]. The wake consists of a series of three-cusped deltoid curves, each formed by the crests of a transverse and two diverging waves (which may not all be always visible). While the size of deltoids is scaled by $\lambda = v^2/g$, where g is the acceleration due to gravity, the cusps' loci form the arms of a ∇ -shaped sector or wedge that enwraps the wake with an opening half-angle of $\varphi_K \approx 19.5^\circ$, independent of the speed. The universality of that pattern is a consequence of the dispersion relation between the frequency ω and the wave number k of the surface gravity waves, given as $\omega = \sqrt{gk}$. The interest in this topic was recently revived by questioning the universality of Kelvin's angle φ_K following a series of empirical observations of ship wakes using Google Earth images [2] and the subsequent debate [3–7].

Similar wake phenomena are studied in atmospheric sciences and oceanography [8–12], and are observed in a diverse range of other areas in physics [13–16]. The study of the wake effect in condensed matter, where it arises in the linear response of electrons to a propagating charged particle, has a long and distinguished history [17–20], which has recently switched its focus on two-dimensional (2D) materials [21–25].

A fascinating analogy between the Kelvins ship wake and the electric potential in a 2D conductor perturbed by a charged particle moving on a parallel trajectory was shown to be a consequence of the identical dispersion, given in the

nonrelativistic limit at long wavelengths by $\omega = \sqrt{g_*k}$ [25]. This relation is a robust manifestation of the long-ranged Coulomb interaction among the charge carriers in a 2D material, which in the simplest case of one energy band crossed by Fermi level [26–28] gives an acceleration at zero temperature as $g_* = 2\pi e^2 |n|/m_*$, where n is the doping density and m_* the effective mass of electrons or holes [29]. This result is obtained by treating the dielectric response of the material in the optical limit [30] and considering the intra-band electron transitions only, which give rise to a Drude conductivity, $\sigma^{\text{intra}}(\omega) = ie^2 |n|/(m_*\omega)$ (neglecting damping) [28,31,32]. Because of the analogy with Kelvin's wake, the wave pattern in the electric potential in the plane of the material may be called the Kelvin-Drude (KD) wake.

While the relation $\omega = \sqrt{g_*k}$ holds for an idealized 2D free-electron gas [24,25,33], it nevertheless describes well the long wavelength dispersion of a low-loss sheet plasmon in graphene and other 2D materials [34] of interest for applications at frequencies from the terahertz to the midinfrared (MIR) [26,27,31]. However, recent studies of a broader class of 2D materials revealed that important modifications may arise to their optical conductivity that can affect their optoelectronic and plasmonic properties in a fundamental way. Accordingly, the patterns of the KD wake in such materials may also be changed in unconventional ways, which may or may not have a counterpart in the fluid mechanics of Kelvin's ship wake.

For example, in the optical conductivity of monolayer transition metal dichalcogenides (TMDs), besides the $\sigma^{\text{intra}}(\omega)$ term, there is a substantial contribution from the interband electron transitions [28,35], which may be well approximated at frequencies much smaller than the typical band gaps in TMDs by $\sigma^{\text{inter}}(\omega) \approx -i\omega\alpha$, where α is an in-plane static polarizability of the material [36–39]. The thus-amended total optical conductivity [40], $\sigma(\omega) = \sigma^{\text{intra}}(\omega) + \sigma^{\text{inter}}(\omega)$, reproduces a plasmon dispersion found in Ref. [28], $\omega = \sqrt{g_*k/(1 + 2\pi\alpha k)}$. This relation exhibits “flattening” for increasing k , which gives rise to “slow plasmons” that were recently suggested in real, quasi-2D metals [28,35]. A similar flattening of the dispersion at short wavelengths is encountered in models for the lee waves excited in the atmosphere

*Also at Waterloo Institute for Nanotechnology, University of Waterloo, Waterloo, Ontario N2L 3G1, Canada; zmiskovi@uwaterloo.ca

Published by the American Physical Society under the terms of the Creative Commons Attribution 4.0 International license. Further distribution of this work must maintain attribution to the author(s) and the published article's title, journal citation, and DOI.

by an air flow around orographic obstacles, such as isolated mountains or islands in the ocean [10,11].

Quite possibly the most exciting modification of the plasmon dispersion occurs in anisotropic 2D materials, such as the doped semiconductor phosphorene [41–43] and the semimetallic WTe_2 [44]. Those materials are naturally occurring realizations of hyperbolic metasurfaces [45–47], which can support a topological transition from elliptic to hyperbolic shapes of isofrequency dispersion curves in the plane of the plasmon wave vectors \mathbf{k} . In the case of doped phosphorene, the anisotropy gives rise to a diagonal optical conductivity tensor, with the components $\sigma_x(\omega)$ and $\sigma_y(\omega)$ along its principal crystalline axes, labeled as the armchair (AC) and the zigzag (ZZ) directions, respectively. The intraband parts of $\sigma_{x/y}(\omega)$ retain the Drude form, given for a single band with damping γ by

$$\sigma_{x/y}^{\text{intra}}(\omega) = i \frac{e^2}{m_{x/y}} \frac{|n|}{\omega + i\gamma}, \quad (1)$$

where the anisotropy of the Drude weights is encoded via the effective electron (or hole) masses, m_x and m_y , in the AC and ZZ directions, respectively [48–51]. On the other hand, the interband electron transitions were shown to play a pivotal role in facilitating a hyperbolic plasmon dispersion to occur in the THz-MIR range [44,52]. In that range, the interband parts of $\sigma_{x/y}(\omega)$ may be approximated similarly to the TMDs [28] by $\sigma_{x/y}^{\text{inter}}(\omega) = -i\omega\alpha_{x/y}$, where α_x and α_y are the components of a static polarizability tensor in phosphorene [37,38,51].

Furthermore, the role of the interband transitions in “flattening” the plasmon dispersion [28,35] is disrupted in some 2D materials by the proximity of the continuum of the intraband electron-hole (e-h) excitations, giving rise to nonlocal effects for increasing k [32,53–55], so that the phase speed of the plasmon attains a minimum at the Fermi speed. This is analogous to the nonlocal effect in the KD wake due to a sound mode in 2D electron liquids [24,25], or to the effect of capillarity in Kelvin’s ship wake [56,57], where the ensuing velocity thresholds for the wave formation give rise to a Mach or Cherenkov type of wake in both systems [16,24,25,56]. Leaving out the sound mode in the hydrodynamic limit of electronic motion in 2D [58], we shall assess the nonlocal effects in the KD wake due to the proximity of the e-h continuum, which is a characteristic of the random phase approximation (RPA) for the intraband electron transitions in a 2D electron gas [36,49,55,59]. For sufficiently large doping density $|n|$, these effects may be well approximated analytically by a semiclassical model [53,54,60,61], which is readily adapted to an anisotropic material [36,37,40,49].

Our primary goal in this article is to elucidate modifications in the KD wake in a generic anisotropic 2D material represented by doped phosphorene [51] and described by an effective 2D dielectric function $\epsilon(\mathbf{k}, \omega)$ [37,62]. We remark that a recent study revealed a quite strong anisotropy in the stopping force on a charged particle moving parallel to doped phosphorene [37], echoing observations related to an equivalent effect of the wave resistance for a ship moving in the presence of a shear current in the water beneath the ship [6,63]. With Kelvin’s ship wake shown to exhibit a prominent shear-induced anisotropy [6,63], it is intriguing to see how the

KD wake in a 2D material is affected by the anisotropy in the effective electron/hole masses, which have no equivalent in fluid mechanics.

II. MODELING

For a particle of charge Q moving with constant velocity \mathbf{v} at distance $z_0 > 0$ above a 2D material that occupies the $z = 0$ plane of a Cartesian coordinate system, the electric potential in that plane at the position $\mathbf{r} = (x, y)$ in the moving frame of reference is [37]

$$\Phi(\mathbf{r}) = \frac{Q}{\pi} \iint_{>} \frac{d^2\mathbf{k}}{k} e^{-kz_0} \Re \left[\frac{e^{i\mathbf{k}\cdot\mathbf{r}}}{\epsilon(\mathbf{k}, \mathbf{k}\cdot\mathbf{v})} \right]. \quad (2)$$

Here, we used the property $\epsilon(-\mathbf{k}, -\omega) = \epsilon^*(\mathbf{k}, \omega)$, where $*$ means complex conjugate, to restrict the integration domain to the half-plane $\mathbf{k}\cdot\mathbf{v} > 0$. Switching to polar coordinates, $\mathbf{k} = (k, \theta)$, with θ taken with respect to the AC direction, we may write for a free-standing material in the optical limit [37]

$$\epsilon(k, \theta, \omega) = 1 + i2\pi \frac{k}{\omega} [\sigma_x(\omega) \cos^2 \theta + \sigma_y(\omega) \sin^2 \theta], \quad (3)$$

where $\sigma_{x/y}(\omega) = \sigma_{x/y}^{\text{intra}}(\omega) + \sigma_{x/y}^{\text{inter}}(\omega)$.

In computations we used parameters deduced from *ab initio* calculations for an electron-doped phosphorene with $n = 10^{13} \text{ cm}^{-2}$ [51], which are listed in the Supplemental Material (SM) [40]. The dielectric function in Eq. (3) with those parameters constitutes what we call the optical model, whereas setting $\alpha_x = \alpha_y = 0$ gives the (anisotropic) Drude model. The details of the semiclassical model are given in the SM [40] and in Ref. [37]. The dependence on the direction of motion of the charged particle enters through the polar form of its velocity, $\mathbf{v} = (v, \theta_0)$, with θ_0 taken with respect to the AC direction. All distances are normalized according to $\bar{x} = x/\ell_c$ and $\bar{y} = y/\ell_c$, where $\ell_c = 2\pi m_0 e^2 / (\hbar^2 n) \approx 1.19 \mu\text{m}$.

Our choice of the scattering geometry is geared toward experiments on electron energy loss spectroscopy (EELS) with aloof electron beams [64–66]. We select the distance to be $z_0 = 50 \text{ nm}$ as a typical value in such experiments and we narrow the parameter space down by choosing the speed of $v = 2v_B$, where $v_B = e^2/\hbar$ is the Bohr speed. Our reason for choosing this speed is to make the Froude number [3,24,56], $\text{Fr} = v/\sqrt{z_0 g}$, take an average value of $\text{Fr} \approx 1$ when the acceleration g is given by $g_d = 2\pi e^2 n/m_d$, where $m_d = \sqrt{m_x m_y}$ is the density of states (DOS) mass of phosphorene [40,48,49]. With such a choice of the parameters pertaining to the incident particle, it is justified to neglect both relativistic effects [67,68] (see also Fig. S10 in the SM [40]) and the quantum mechanical wavelength of the incident electron [66] in the wake potential.

Important information on the wake patterns in the far-field region of the $\mathbf{r} = (x, y)$ plane is revealed by the method of stationary phase [6,11,25] while taking into account the singularities in the integral in Eq. (2). The curves with constant phase are obtained from the critical points of $f = \mathbf{k}\cdot\mathbf{r}$ in Eq. (2) with fixed \mathbf{r} , subject to the constraint $\epsilon(\mathbf{k}, \mathbf{k}\cdot\mathbf{v}) = 0$. This is equivalent to solving the equation $\epsilon(\mathbf{k}, \omega) = 0$ in the absence of damping to obtain the plasmon frequency $\omega = \omega_p(\mathbf{k})$ while imposing the radiation condition, $\omega_p(\mathbf{k}) = \mathbf{k}\cdot\mathbf{v}$.

Then, the curves of constant phase f are obtained as [11]

$$\mathbf{r} = f \frac{\mathbf{v}_g(\mathbf{k}) - \mathbf{v}}{\mathbf{k} \cdot \mathbf{v}_g(\mathbf{k}) - \omega_p(\mathbf{k})}, \quad (4)$$

where $\mathbf{v}_g(\mathbf{k}) = \partial\omega_p(\mathbf{k})/\partial\mathbf{k}$ is the plasmon group velocity. In the SM [40], we show how the right-hand side of Eq. (4) may be written in polar coordinates, $\mathbf{k} = (k, \theta)$, see Eqs. (S17) and (S18) in the SM [40]. All our models of the dielectric function yield analytic expressions for $\omega_p(k, \theta)$, see Eqs. (S11), (S14), and (S15) in the SM [40], and they allow for an explicit solution of the corresponding radiation conditions $\omega_p(k, \theta) = kv \cos(\theta - \theta_0)$ in the form $k = k_r(\theta)$. Upon inserting those expressions in the right-hand side of Eq. (4), one achieves a parametrization of the coordinates x and y on isophase curves in terms of angle $\theta \in (\theta_0 - \frac{\pi}{2}, \theta_0 + \frac{\pi}{2})$. Then, analyzing the extremal points in the slope function $S(\theta) = -y/x$ can be used to deduce the opening angles φ_w of wedges enclosing different types of waves in the wake, taken with respect to the direction opposite to \mathbf{v} [63].

III. RESULTS

In Fig. 1, we show the density plots of the wake potential in doped phosphorene for three directions of motion of a charged particle with $v = 2v_B$. In the AC direction, Fig. 1(a), characterized by a light electron mass m_x , the wake is dominated by transverse waves that are concave-shaped relative to the direction of motion, which is opposite from the typical convex shape of transverse waves in the classic Kelvin's wake [11,24,25,56]. The half-opening angle of the wedge enclosing the wake is found from the stationary phase analysis [40] as $\varphi_{AC} \approx 23.8^\circ$, somewhat larger than $\varphi_K \approx 19.5^\circ$. In the ZZ direction, Fig. 1(c), characterized by a heavy electron mass m_y , the wake is dominated by diverging waves, enclosed by a wedge with a quite larger half-angle of $\varphi_{ZZ} \approx 57.2^\circ$. While the stationary phase analysis shows that the wakes consist of both the transverse and diverging waves, as well as hybrid waves in the AC direction (see below), some of those waves are suppressed depending on the Froude number, $Fr = v/\sqrt{z_0 g}$. For Kelvin's wake, it was shown that the transverse waves dominate for small, $Fr < 1$, while the diverging waves dominate for large, $Fr > 1$, values [3,24,56]. Evaluating the Froude number with $g_{x/y} = 2\pi e^2 |n|/m_{x/y}$ using our parameters [40] gives $Fr \approx 0.57$ in the AC direction and $Fr \approx 1.64$ in the ZZ direction, explaining the observed types of waves in Figs. 1(a) and 1(c).

The most intriguing wake pattern occurs in Fig. 1(b) for the direction with $\theta_0 = \pi/4$, midway between the AC and ZZ directions. The wake is dominated by diverging waves, which show a marked anisotropy with respect to the direction of motion of the charged particle, with a wedge having the opening angles of $\varphi_{\text{right}} \approx 82.7^\circ$ and $\varphi_{\text{left}} \approx 23.9^\circ$ to the right (toward AC) and left (toward ZZ), respectively. This wake asymmetry is quite similar to the asymmetry found in Kelvin's ship wake in the presence of a sideways shear current [6,63] (see, e.g., Fig. 4 in Ref. [6]). In the case of the KD wake, the asymmetry in the far-field region is dominated by the asymmetry of the effective electron masses in the Drude model. Thus, we analyze in Fig. 2 the isophase curves from an

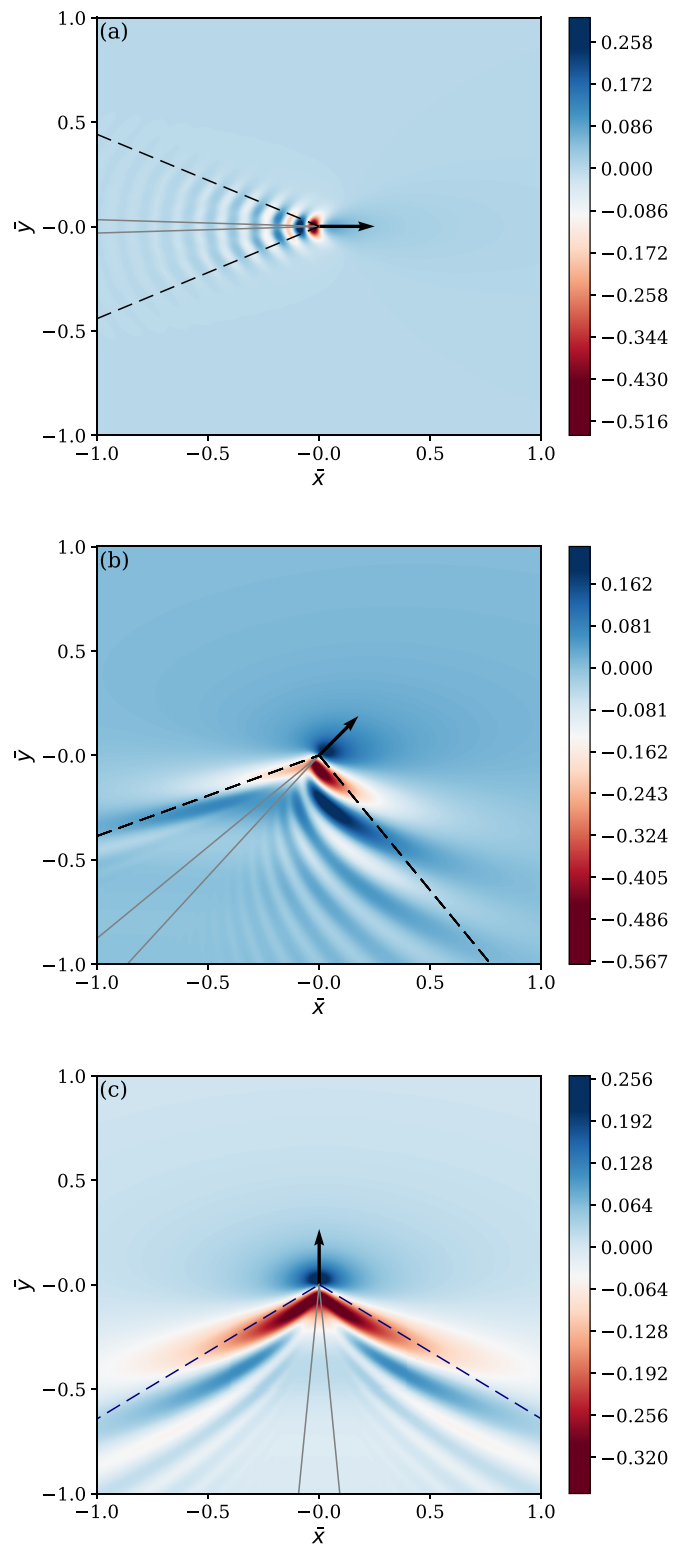


FIG. 1. The normalized wake potential, Φ_{z_0}/Q^2 , in doped phosphorene as a function of the normalized coordinates \bar{x} (AC axis) and \bar{y} (ZZ axis) from semiclassical model for three directions of motion, indicated by the arrows with (a) $\theta_0 = 0$, (b) $\theta_0 = \pi/4$, and (c) $\theta_0 = \pi/2$, for a particle moving at distance $z_0 = 50$ nm with the speed $v = 2v_B$. The dashed black lines define the wedge enclosing the KD wake, while the solid gray lines are the asymptotes of the fan waves, defining the Mach-like wedge, see Fig. 3.

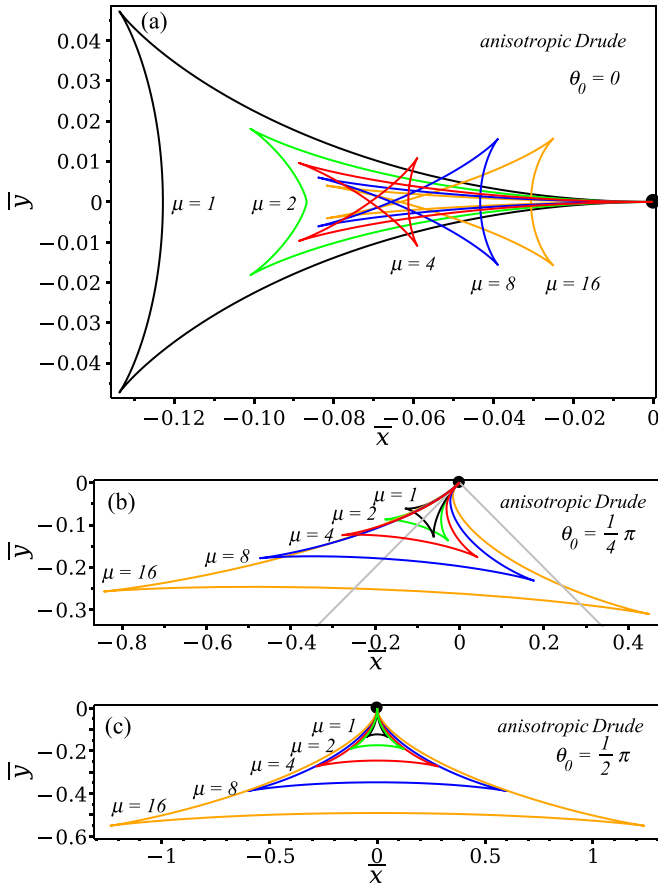


FIG. 2. The isophase curves with $f = -\pi$ in coordinates \bar{x} (AC axis) and \bar{y} (ZZ axis) using the Drude model of anisotropic material with fixed DOS mass $m_d = \sqrt{m_x m_y}$ and variable ratio $\mu = m_y/m_x$ taking values of 1 (black), 2 (green), 4 (red), 8 (blue), and 16 (orange) for $v = 2v_B$ and three directions of motion with (a) $\theta_0 = 0$, (b) $\theta_0 = \pi/4$, and (c) $\theta_0 = \pi/2$. The gray lines in (b) show the axes rotated through $\theta_0 = \pi/4$.

anisotropic Drude model having the DOS mass m_d fixed by the phosphorene data [51], while letting the anisotropy ratio $\mu = m_y/m_x$ be a variable parameter. Notice that the isotropic Drude limit with $\mu = 1$ gives rise to a black deltoid curve in Fig. 2, which is the classic Kelvin’s pattern consisting of two diverging waves and one convex transverse wave.

One sees in Fig. 2(a) that the transverse and diverging waves no longer meet at the same pair of cusps when $\mu > 2$. Rather, there emerge two new branches, which we call hybrid because they connect the endpoints of the transverse wave with the endpoints of diverging waves on the opposite sides of the wake. As a result, Fig. 2(a) shows that for $\theta_0 = 0$ the three-cusped Kelvin’s deltoid undergoes a topological transition to a five-cusped pentacle at $\mu = 2$ [40]. The loci of the endpoints of the hybrid branches now define two wedges, one enclosing a concave transverse wave, which dominates the wake in Fig. 1(a), and the other wedge that encloses the diverging waves. In Figs. 2(b) and 2(c), the KD wake retains a deltoid form, which grows in size and broadens with increasing μ [69], while getting asymmetrically distorted for $\theta_0 = \pi/4$ in Fig. 2(b). Interestingly, one sees in Fig. 2(b) that the diverging wave in the wake with $\mu = 16$ [70] precedes the position of

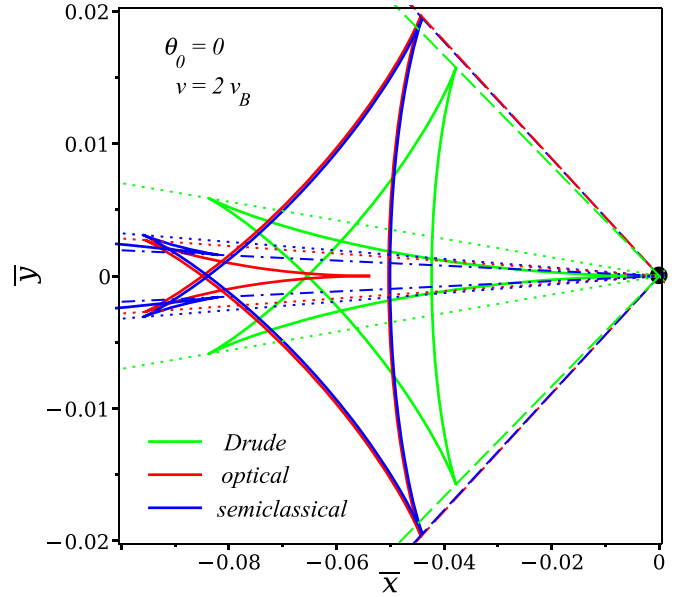


FIG. 3. The isophase curves (solid lines) with $f = -\pi$ in normalized coordinates \bar{x} (AC axis) and \bar{y} (ZZ axis) using the Drude model (green), optical model (red), and semiclassical model (blue) of doped phosphorene for a particle moving in the AC direction ($\theta_0 = 0$) at the speed $v = 2v_B$. The dashed and dotted lines indicate the wedges enclosing the transverse and diverging waves, respectively, while the dash-dotted lines pass through the cusps where “fan” waves get detached from the diverging waves in the semiclassical model.

the particle on the side toward the AC direction. Similarly, one of the wedge angles in Kelvin’s ship wake was also found to exceed $\pi/2$ for a strong side-on shear current [6].

It should be noted that the shape of the wake patterns in the anisotropic Drude model is independent of the particle speed [40]. Namely, in analogy with the classic Kelvin wake, the size of the isophase curves in Fig. 2 can be scaled with $\lambda = v^2/g_d$, which removes the dependence on v when the coordinates are expressed in the normalized form $\bar{x} = x/\lambda$ and $\bar{y} = y/\lambda$ (see Figs. S3–S5 in the SM [40]). On the other hand, while the optical and semiclassical models yield wake patterns that approach those of the Drude model as the speed increases, they exhibit a remarkable evolution of shapes of the isophase curves at low speeds, $v < v_B$, as shown in Fig. S5 in the SM [40]. Studying those effects requires more advanced models of the dielectric function to describe nonlocal effects at low speeds, going beyond the scope of this work.

The largest differences between the three dielectric models of doped phosphorene are observed for the particle motion in the AC direction, which are discussed in Fig. 3 by juxtaposing three isophase curves. Compared with the Drude model (green), the main effect of the interband part in the optical model (red) is to move the central cusp in the pentacle where the diverging waves meet to a position way behind the particle (see Fig. 8 in Ref. [11] and Sec. S4 in the SM [40]), while still exhibiting two wedges that enclose the transverse (dashed) and diverging (dotted) waves. On the other hand, the isophase curve in the semiclassical model (blue) follows closely the curve in the optical model, excepting the region of the cusp where the diverging waves meet, which is broken by the

emergence of a pair of “fan” waves [57] due to nonlocal effects. Those fan branches extend asymptotically to infinity behind the particle, forming a Mach-like wedge (gray lines in Fig. 1) with opening angles defined by a direction-dependent threshold for the particle speed due to the e-h continuum (Eq. (S19) in the SM [40]). The fan branches meet the diverging branches at a pair of cusps that define a new wedge (dash-dotted) in Fig. 3 in a manner similar to the structures revealed in recent studies of capillary-gravity wakes (see, e.g., Fig. 7 in Ref. [56] or Fig. 8 in Ref. [57]).

IV. CONCLUSION

By using three dielectric response models that were established in recent studies of hyperbolic plasmons in anisotropic 2D materials and slow plasmons in quasi-2D metals, we displayed a diverse set of wake structures in the potential induced by the passage of a charged particle. By taking advantage of analytical tractability of our dielectric response models, we performed a detailed stationary phase analysis, enabling us to identify unexpected analogies in the shape of the wake patterns in those materials with similar effects observed in the macroscopic ship and atmospheric wakes regarding the asymmetry (due to shear currents), flattening of the dispersion (in the orographic lee waves), and the Mach-like wakes (due to capillarity), even though the microscopic origins of those effects in 2D materials are quite different from those in the macroscopic wakes.

While our modeling is suited for the scattering geometry in EELS with an aloof electron beam of medium energy [64,65], the displayed wake patterns may be difficult to observe in such a setting because of the fast time scales and the short length scales in the response of the 2D target materials. A possible alternate scenario would involve a static obstacle in the presence of an electron flow in the material, like in the recent experiment [71]. While this experiment agrees with the hydrodynamic limit of the electron motion in 2D [58], it also points to a need to extend the present study of the wake effect to low (relative) speeds, where the wake patterns are strongly affected by the plasmon dispersion at increasing wave numbers. In that context, exploring various analytical models of the electron dynamics in both the hydrodynamic and RPA regimes would be of interest for extending the stationary-phase analysis to speeds near the velocity threshold for the wake formation. Such an analysis could yield valuable insight into the directionality of plasmon excitation in anisotropic 2D materials and the role of nonlocal effects.

ACKNOWLEDGMENTS

The authors acknowledge helpful input from M. R. Preciado Rivas in the early stages of this project. This work was supported by the Natural Sciences and Engineering Research Council of Canada (Grant No. 2023-03397).

-
- [1] L. Kelvin, On ship waves, *Proc. Inst. Mech. Eng.* **38**, 409 (1887).
 - [2] M. Rabaud and F. Moisy, Ship Wakes: Kelvin or Mach Angle? *Phys. Rev. Lett.* **110**, 214503 (2013).
 - [3] A. Darmon, M. Benzaquen, and E. Raphaël, Kelvin wake pattern at large Froude numbers, *J. Fluid Mech.* **738**, R3 (2014).
 - [4] F. Noblesse, J. He, Y. Zhu, L. Hong, C. Zhang, R. Zhu, and C. Yang, Why can ship wakes appear narrower than Kelvin’s angle? *Eur. J. Mech. B Fluids* **46**, 164 (2014).
 - [5] R. Pethiyagoda, S. W. McCue, and T. J. Moroney, What is the apparent angle of a Kelvin ship wave pattern? *J. Fluid Mech.* **758**, 468 (2014).
 - [6] S. Å. Ellingsen, Ship waves in the presence of uniform vorticity, *J. Fluid Mech.* **742**, R2 (2014).
 - [7] J. Colen and E. B. Kolomeisky, Kelvin-Froude wake patterns of a traveling pressure disturbance, *Eur. J. Mech. B Fluids* **85**, 400 (2021).
 - [8] C. Schär and R. B. Smith, Shallow-water flow past isolated topography. Part I: Vorticity production and wake formation, *J. Atmos. Sci.* **50**, 1373 (1993).
 - [9] I. Ginis and G. Sutyryn, Hurricane-generated depth-averaged currents and sea surface elevation, *J. Phys. Oceanogr.* **25**, 1218 (1995).
 - [10] M. Wurtele, R. Sharman, and A. Datta, Atmospheric lee waves, *Annu. Rev. Fluid Mech.* **28**, 429 (1996).
 - [11] P. N. Svirskunov and M. V. Kalashnik, Phase patterns of dispersive waves from moving localized sources, *Phys. Usp.* **57**, 80 (2014).
 - [12] R. B. Smith, 100 years of progress on mountain meteorology research, *Meteorol. Monogr.* **59**, 20.1 (2019).
 - [13] O. Ishihara and S. V. Vladimirov, Wake potential of a dust grain in a plasma with ion flow, *Phys. Plasmas* **4**, 69 (1997).
 - [14] H. Suk, N. Barov, J. B. Rosenzweig, and E. Esarey, Plasma Electron Trapping and Acceleration in a Plasma Wake Field Using a Density Transition, *Phys. Rev. Lett.* **86**, 1011 (2001).
 - [15] S. Wang, X. Shan, U. Patel, X. Huang, J. Lu, J. Li, and N. Tao, Label-free imaging, detection, and mass measurement of single viruses by surface plasmon resonance, *Proc. Natl. Acad. Sci. USA* **107**, 16028 (2010).
 - [16] I. Carusotto and G. Rousseaux, The Cerenkov effect revisited: From swimming ducks to zero modes in gravitational analogues, in *Analogue Gravity Phenomenology: Analogue Spacetimes and Horizons, from Theory to Experiment*, edited by D. Faccio, F. Belgiorno, S. Cacciatori, V. Gorini, S. Liberati, and U. Moschella (Springer International Publishing, Cham, 2013), pp. 109–144.
 - [17] V. N. Neelavathi, R. H. Ritchie, and W. Brandt, Bound Electron States in the Wake of Swift Ions in Solids, *Phys. Rev. Lett.* **33**, 302 (1974).
 - [18] F. J. García de Abajo and P. M. Echenique, Wake potential in the vicinity of a surface, *Phys. Rev. B* **46**, 2663 (1992).
 - [19] I. Abril, R. Garcia-Molina, C. D. Denton, F. J. Pérez-Pérez, and N. R. Arista, Dielectric description of wakes and stopping powers in solids, *Phys. Rev. A* **58**, 357 (1998).
 - [20] A. Schinner and P. Sigmund, Polarization wake of penetrating ions: Oscillator model, *Eur. Phys. J. D* **66**, 1 (2012).

- [21] D. J. Mowbray, Z. L. Miskovic, F. O. Goodman, and Y.-N. Wang, Wake effect in interactions of fast ions with carbon nanotubes, *Phys. Lett. A* **329**, 94 (2004).
- [22] I. Radovic, D. Borka, and Z. L. Mikovic, Wake effect in doped graphene due to moving external charge, *Phys. Lett. A* **375**, 3720 (2011).
- [23] X. Shi, X. Lin, F. Gao, H. Xu, Z. Yang, and B. Zhang, Causitic graphene plasmons with Kelvin angle, *Phys. Rev. B* **92**, 081404(R) (2015).
- [24] A. J. Chaves, N. M. R. Peres, G. Smirnov, and N. A. Mortensen, Hydrodynamic model approach to the formation of plasmonic wakes in graphene, *Phys. Rev. B* **96**, 195438 (2017).
- [25] E. B. Kolomeisky and J. P. Straley, Kelvin-Mach Wake in a Two-Dimensional Fermi Sea, *Phys. Rev. Lett.* **120**, 226801 (2018).
- [26] F. H. L. Koppens, D. E. Chang, and F. J. García de Abajo, Graphene plasmonics: A platform for strong light-matter interactions, *Nano Lett.* **11**, 3370 (2011).
- [27] T. Low and P. Avouris, Graphene plasmonics for terahertz to mid-infrared applications, *ACS Nano* **8**, 1086 (2014).
- [28] F. H. da Jornada, L. Xian, A. Rubio, and S. G. Louie, Universal slow plasmons and giant field enhancement in atomically thin quasi-two-dimensional metals, *Nat. Commun.* **11**, 1013 (2020).
- [29] For graphene, m_* is replaced by $\hbar k_F/v_F$ [72], where $k_F = \sqrt{\pi}|n|$ is its Fermi wave number and $v_F \approx c/300$ its Fermi speed, c being the speed of light.
- [30] The optical limit of the longitudinal response of a 2D material may be formally derived by combining the continuity equation for its charge carriers with Ohm's law using an in-plane conductivity in local form, $\sigma(\omega)$, where one lets $k \rightarrow 0$ [32].
- [31] M. Jablan, H. Buljan, and M. Soljačić, Plasmonics in graphene at infrared frequencies, *Phys. Rev. B* **80**, 245435 (2009).
- [32] V. Despoja, T. Djordjevic, L. Karbunar, I. Radovic, and Z. L. Miskovic, Ab initio study of the electron energy loss function in a graphene-sapphire-graphene composite system, *Phys. Rev. B* **96**, 075433 (2017).
- [33] A. L. Fetter, Electrodynamics of a layered electron gas. I. Single layer, *Ann. Phys.* **81**, 367 (1973).
- [34] Y. Li, Z. Li, C. Chi, H. Shan, L. Zheng, and Z. Fang, Plasmonics of 2D nanomaterials: Properties and applications, *Advanced Sci.* **4**, 1600430 (2017).
- [35] C. Song, X. Yuan, C. Huang, S. Huang, Q. Xing, C. Wang, C. Zhang, Y. Xie, Y. Lei, F. Wang *et al.*, Plasmons in the van der Waals charge-density-wave material 2H-TaSe₂, *Nat. Commun.* **12**, 386 (2021).
- [36] M. N. Gjerding, L. S. R. Cavalcante, A. Chaves, and K. S. Thygesen, Efficient ab initio modeling of dielectric screening in 2D van der Waals materials: Including phonons, substrates, and doping, *J. Phys. Chem. C* **124**, 11609 (2020).
- [37] M. Moshayedi, M. R. P. Rivas, and Z. L. Mišković, Stopping and image forces on a charged particle moving parallel to an anisotropic two-dimensional material, *Phys. Rev. B* **105**, 075429 (2022).
- [38] Z. L. Miskovic, M. Moshayedi, M. R. P. Rivas, J. Jakovac, I. Radovic, and V. Despoja, Modeling of the interband transitions in the optical conductivity of doped two-dimensional materials in the terahertz to the infrared frequency range: The case studies of graphene and phosphorene, *Radiat. Eff. Defects Solids* **178**, 54 (2023).
- [39] In the absence of intraband transitions, this approximation gives rise to the Rytova-Keldysh model dielectric function that is often used to describe static screening of the Coulomb interaction for computations of the exciton bound states in 2D semiconductors [73,74].
- [40] See Supplemental Material at <http://link.aps.org/supplemental/10.1103/PhysRevResearch.5.033133> for further details on (SI) the three dielectric models and (SII) the stationary phase analysis, which is focused on (S1) comparison between the three models at medium-to-high and low speeds, (S2) Mach-like wake due to nonlocal effects, (S3) opening angles of wedges containing KD wakes, (S4) slow isotropic plasmons, and (S5) relativistic effects.
- [41] F. Xia, H. Wang, and Y. Jia, Rediscovering black phosphorus: A unique anisotropic 2D material for optoelectronics and electronics, *Nat. Commun.* **5**, 4458 (2014).
- [42] T. Low, A. S. Rodin, A. Carvalho, Y. Jiang, H. Wang, F. Xia, and A. H. Castro Neto, Tunable optical properties of multilayer black phosphorus thin films, *Phys. Rev. B* **90**, 075434 (2014).
- [43] X. Wang and S. Lan, Optical properties of black phosphorus, *Adv. Opt. Photonics* **8**, 618 (2016).
- [44] C. Wang, S. Huang, Q. Xing, Y. Xie, C. Song, F. Wang, and H. Yan, Van der Waals thin films of WTe₂ for natural hyperbolic plasmonic surfaces, *Nat. Commun.* **11**, 1158 (2020).
- [45] J. S. Gomez-Diaz and A. Alù, Flatland optics with hyperbolic metasurfaces, *ACS Photonics* **3**, 2211 (2016).
- [46] P. Huo, S. Zhang, Y. Liang, Y. Lu, and T. Xu, Hyperbolic metamaterials and metasurfaces: Fundamentals and applications, *Adv. Opt. Mater.* **7**, 1801616 (2019).
- [47] G. Jia, J. Luo, H. Wang, Q. Ma, Q. Liu, H. Dai, and R. Asgari, Two-dimensional natural hyperbolic materials: From polaritons modulation to applications, *Nanoscale* **14**, 17096 (2022).
- [48] T. Low, R. Roldán, H. Wang, F. Xia, P. Avouris, L. M. Moreno, and F. Guinea, Plasmons and Screening in Monolayer and Multilayer Black Phosphorus, *Phys. Rev. Lett.* **113**, 106802 (2014).
- [49] S. Ahn and S. Das Sarma, Theory of anisotropic plasmons, *Phys. Rev. B* **103**, L041303 (2021).
- [50] S. Biswas, W. S. Whitney, M. Y. Grajower, K. Watanabe, T. Taniguchi, H. A. Bechtel, G. R. Rossman, and H. A. Atwater, Tunable intraband optical conductivity and polarization-dependent epsilon-near-zero behavior in black phosphorus, *Sci. Adv.* **7**, eabd4623 (2021).
- [51] D. Novko, K. Lyon, D. J. Mowbray, and V. Despoja, Ab initio study of electromagnetic modes in two-dimensional semiconductors: Application to doped phosphorene, *Phys. Rev. B* **104**, 115421 (2021).
- [52] A. Nemilentsau, T. Low, and G. Hanson, Anisotropic 2D Materials for Tunable Hyperbolic Plasmonics, *Phys. Rev. Lett.* **116**, 066804 (2016).
- [53] G. Lovat, G. W. Hanson, R. Araneo, and P. Burghignoli, Semi-classical spatially dispersive intraband conductivity tensor and quantum capacitance of graphene, *Phys. Rev. B* **87**, 115429 (2013).
- [54] D. Correas-Serrano, J. Gomez-Diaz, M. Tymchenko, and A. Alù, Nonlocal response of hyperbolic metasurfaces, *Opt. Express* **23**, 29434 (2015).
- [55] R. Petersen, T. G. Pedersen, and F. Javier García de Abajo, Nonlocal plasmonic response of doped and optically pumped graphene, MoS₂, and black phosphorus, *Phys. Rev. B* **96**, 205430 (2017).

- [56] F. Moisy and M. Rabaud, Mach-like capillary-gravity wakes, *Phys. Rev. E* **90**, 023009 (2014).
- [57] H. Liang and X. Chen, Asymptotic analysis of capillary-gravity waves generated by a moving disturbance, *Eur. J. Mech. B Fluids* **72**, 624 (2018).
- [58] A. Lucas and K. C. Fong, Hydrodynamics of electrons in graphene, *J. Phys.: Condens. Matter* **30**, 053001 (2018).
- [59] F. Stern, Polarizability of a Two-Dimensional Electron Gas, *Phys. Rev. Lett.* **18**, 546 (1967).
- [60] I. Radovic, L. Hadzievski, and Z. L. Miskovic, Polarization of supported graphene by slowly moving charges, *Phys. Rev. B* **77**, 075428 (2008).
- [61] D. Svintsov and V. Ryzhii, Comment on “Negative Landau Damping in Bilayer Graphene,” *Phys. Rev. Lett.* **123**, 219401 (2019).
- [62] A. M. Holmes and G. W. Hanson, Conditions for photonic band gaps in two-dimensional materials, *J. Appl. Phys.* **129**, 015302 (2021).
- [63] Y. Li and S. Å. Ellingsen, Ship waves on uniform shear current at finite depth: Wave resistance and critical velocity, *J. Fluid Mech.* **791**, 539 (2016).
- [64] P. A. Crozier, Vibrational and valence aloof beam eels: A potential tool for nondestructive characterization of nanoparticle surfaces, *Ultramicroscopy* **180**, 104 (2017).
- [65] G. Radtke, D. Taverna, N. Menguy, S. Pandolfi, A. Courac, Y. Le Godec, O. L. Krivanek, and T. C. Lovejoy, Polarization Selectivity in Vibrational Electron-Energy-Loss Spectroscopy, *Phys. Rev. Lett.* **123**, 256001 (2019).
- [66] Y. Adiv, H. Hu, S. Tsesses, R. Dahan, K. Wang, Y. Kurman, A. Gorlach, H. Chen, X. Lin, G. Bartal *et al.*, Observation of 2D Cherenkov Radiation, *Phys. Rev. X* **13**, 011002 (2023).
- [67] Z. L. Miskovic, K. Akbari, S. Segui, J. L. Gervasoni, and N. R. Arista, Relativistic effects in the energy loss of a fast charged particle moving parallel to a two-dimensional electron gas, *Nucl. Instrum. Methods Phys. Res., Sect. B* **422**, 18 (2018).
- [68] K. Akbari and Z. L. Miskovic, Directional effects in plasmon excitation and transition radiation from an anisotropic 2D material induced by a fast charged particle, *Nanoscale* **14**, 5079 (2022).
- [69] The shrinking of the wake in Fig. 2(a) and its increase in Fig. 2(c) with increasing μ may be explained by defining a direction-dependent scaling length of the isophase curves for anisotropic Drude model as $\lambda(\theta) = v^2/g(\theta)$, where $g(\theta) = g_d(\sqrt{\mu} \cos^2 \theta + \sin^2 \theta / \sqrt{\mu})$ with $g_d = 2\pi e^2 n / m_d$ [40]. Then, $\lambda(0) \propto 1/\sqrt{\mu}$ and $\lambda(\pi/2) \propto \sqrt{\mu}$.
- [70] $\mu \approx 8.4$ for phosphorene [40].
- [71] Z. J. Krebs, W. A. Behn, S. Li, K. J. Smith, K. Watanabe, T. Taniguchi, A. Levchenko, and V. W. Brar, Imaging the breaking of electrostatic dams in graphene for ballistic and viscous fluids, *Science* **379**, 671 (2023).
- [72] S. H. Abedinpour, G. Vignale, A. Principi, M. Polini, W.-K. Tse, and A. H. MacDonald, Drude weight, plasmon dispersion, and ac conductivity in doped graphene sheets, *Phys. Rev. B* **84**, 045429 (2011).
- [73] P. Cudazzo, I. V. Tokatly, and A. Rubio, Dielectric screening in two-dimensional insulators: Implications for excitonic and impurity states in graphene, *Phys. Rev. B* **84**, 085406 (2011).
- [74] A. S. Rodin, A. Carvalho, and A. H. Castro Neto, Excitons in anisotropic two-dimensional semiconducting crystals, *Phys. Rev. B* **90**, 075429 (2014).